Two-dimensional prognostic experiments for fast-flowing ice streams from the Academy of Sciences Ice Cap

Y V Konovalov, O V Nagornov

National Research Nuclear University MEPhI (Moscow Engineering Physics Institute), Kashirskoe shosse, 31, 115409, Moscow, Russian Federation

Abstract. The prognostic experiments for fast-flowing ice streams on the southern side of the Academy of Sciences Ice Cap in the Komsomolets Island, Severnaya Zemlya archipelago, are implemented in this study. These experiments are based on inversions of basal friction coefficients using a two-dimensional flow-line thermo-coupled model and the Tikhonov's regularization method. The modeled ice temperature distributions in the cross-sections were obtained using the ice surface temperature histories that were inverted previously from the borehole temperature profile derived at the summit of the Academy of Sciences Ice Cap and employing elevational gradient of ice surface temperature changes, which is equal to about 6.5 ^{0}C km^{-1}. Input data included InSAR ice surface velocities, ice surface elevations, and ice thicknesses obtained from airborne measurements and the surface mass balance, were adopted from previous investigations for the implementation of both the forward and inverse problems. The prognostic experiments reveal that both ice mass and ice stream extents decline for the reference time-independent surface mass balance. Specifically, the grounding line retreats (a) along the B–B′ flow line from ~40 km to ~30 km (the distance from the summit), (b) along the C–C′ flow line from ~43 km to ~37 km, and (c) along the D–D′ flow line from ~41 km to ~32 km considering a time period of 500 years and assuming time-independent surface mass balance. Ice flow velocities in the ice streams decrease with time and this trend results in the overall decline of the outgoing ice flux. Generally, the modeled evolution is in agreement with observations of deglaciation of Severnaya Zemlya archipelago.

1. Introduction

There are relevant diagnostic observations of glaciers such as digital Landsat imagery and satellite synthetic aperture radar interferometry (InSAR), airborne measurements, borehole ice temperature and ice surface mass balance measurements. These observations provide data for prognostic experiments that allow prediction of future glacier conditions for different climatic scenarios in the future. These experiments can be performed employing the mathematical modeling and in this study a two-dimensional ice flow model is applied for prediction of the future conditions of fast-flowing ice streams on the southern side of the Academy of Sciences Ice Cap in the Komsomolets Island, Severnaya Zemlya archipelago (figure 1 of [1]).

The observations were based on digital Landsat imagery and satellite synthetic aperture radar interferometry (InSAR) and revealed four drainage basins and four fast-flowing ice streams on the southern side of the Academy of Sciences Ice Cap in the Komsomolets Island, Severnaya Zemlya archipelago (figure 10 of [1]). The four ice streams are 17–37 km long and 4–8 km wide [1]. Bedrock elevations of these areas are below the sea level, and the ice flow velocities attain a value of 70–140 m/a (figure 10 of [1]). Such fast flow-line features are typical for outlet glaciers and ice streams in

both the Arctic and the Antarctic. These ice streams are the major locations of iceberg calving from the Academy of Sciences Ice Cap [1].

The flow-line profiles of the three ice streams on the southern side of the Academy of Sciences Ice Cap are shown in figure 8 of [1]. Ice flow in these ice streams is simulated with a two-dimensional flow-line higher-order finite-difference model, e.g., [2]-[4]. This model describes an ice flow along a flow line [3], [4]. The results of the diagnostic experiments obtained in [5], for instance, for the C–C′ flow-line profile show that the ice surface velocity along the flow line attains a value of 100 m/a assuming that ice is sliding. However, the observed surface velocity distribution along the C–C′ flow-line profile [1] is not similar to that obtained by the model experiments for constant values of friction coefficient and for both linear and nonlinear friction laws [5]. Similarly, the diagnostic experiments carried out for the B–B′ and D–D′ profile data show the same results for the ice flow velocities. The deviation between the observed and modeled surface velocities suggests that the friction coefficient should be a spatially variable parameter. Therefore, to achieve a better agreement between the observed and simulated velocities, the spatial distribution of the friction coefficients requires to be optimized and an inverse problem needs to be solved, e.g., [6]-[14].

The inversion of friction coefficients is based on the minimization of the deviation between the observed and modeled surface velocities. A series of test experiments [5], in which modeled surface velocities are used as observations in the inverse problem, have shown that the inverse problem for the full 2D ice flow-line model is ill posed. More precisely, the surface velocity is weakly sensitive to small perturbations in friction coefficients, and as a result the perturbations appear in the inverted friction coefficients [5].

Herein, in the prognostic experiments we use the friction coefficients inversions obtained by applying the Tikhonov's regularization method, in which Tikhonov's stabilizing functional is added to the main discrepancy functional [15].

The inversions of friction coefficient are used in the prognostic experiments for the fast-flowing ice streams. The considered 2D prognostic experiments are the numerical simulations with the ice thickness distribution changes performed by the 2D flow-line thermo-coupled model, which includes diagnostic equations as the heat-transfer equation and the mass-balance equation [3], [4]. In this study, we present the results of the prognostic experiments performed for the B–B′, C–C′, and D–D′ profiles (figure 8 of [1]). Specifically, the prognostic experiments are carried out for the three ice streams (figure 10 of [1]) that are the main sources of the ice flux from the ice cap to the ocean. The results of the prognostic experiments include future modeled histories of ice thickness distributions along the flow lines of grounding line locations and outgoing ice fluxes. The surface mass balance in the performed experiments is considered as time-independent, so the prognostic experiments show the assessment of the minimal ice mass loss in the ice streams in the future, because the obtained forecasts don't include for future global warming. Nevertheless, the results of the prognostic experiments are in agreement with the observations of ice mass loss on the Severnaya Zemlya archipelago [16].

2. Field equations

2.1. Forward problem: Diagnostic equations

The 2D flow-line higher-order model includes the continuity equation for incompressible medium, the mechanical equilibrium equation in terms of stress deviator components [3], [4], and the rheological Glen law [17]:

$$\begin{cases} \int\limits_{h_b}^{z} \dfrac{\partial u}{\partial x}\, dz' + \dfrac{1}{b}\dfrac{d\,b}{d\,x}\int\limits_{h_b}^{z} u\, dz' + w - w_b = 0, \\ 2\dfrac{\partial \sigma'_{xx}}{\partial x} + \dfrac{\partial \sigma'_{yy}}{\partial x} + \dfrac{\partial^2}{\partial x^2}\int\limits_{z}^{h_s} \sigma'_{xz}\, dz + \dfrac{\partial \sigma'_{xz}}{\partial z} = \rho\, g\, \dfrac{\partial h_s}{\partial x}, \\ \sigma'_{ik} = 2\eta\, \dot{\varepsilon}_{ik}; \quad \eta = \dfrac{1}{2}\left(m\, A(T)\right)^{-\frac{1}{n}} \dot{\varepsilon}^{\frac{1-n}{n}}, \\ 0 < x < L; \;\; h_b(x) < z < h_s(x), \end{cases} \tag{1}$$

where (x,z) is a rectangular coordinate system with the x-axis along the flow line and the z-axis pointing vertically upward; u, w are the horizontal and vertical ice flow velocities, respectively; b is the width along the flow-line, σ'_{ik} is the stress deviator; $\dot{\varepsilon}_{ik}$ is the strain-rate tensor; $\dot{\varepsilon}$ is the second invariant of the strain-rate tensor; ρ is the ice density; g is the gravitational acceleration; η is the ice effective viscosity; $A(T)$ is the flow-law rate factor; T is the ice temperature; $h_b(x)$, $h_s(x)$ are the ice bed and ice surface elevations, respectively; and L is the glacier length.

The boundary conditions and some complementary experiments that were carried out applying this model, were considered in [5]. In particular, the technique, when the boundary conditions are included in the momentum equations [5], was applied in the considered here prognostic experiments.

2.2. Inverse problem for the friction coefficient

The inversion of friction coefficient has been carried out using the gradient minimization procedure for the "smoothing" functional [15].

The details of the gradient minimization procedure and the problem of the regularization parameter choice are discussed in [18], [19], [5]. In this manuscript the inversions have been obtained for the linear (viscous) friction law, implying the experiments implemented in [5] with the inversions for the C-C' profile, that have shown a good agreement between the observed (u_{obs}) and the calculated (u_{mod}) surface velocities for the linear friction law.

2.3. Prognostic equations

The thermo-coupled prognostic experiments imply that the 2D flow-line model includes the heat-transfer equation [3], [4]:

$$\frac{\partial T}{\partial t} = \chi\left(\frac{\partial^2 T}{\partial x^2} + \frac{1}{b}\frac{d\,b}{d\,x}\frac{\partial T}{\partial x} + \frac{\partial^2 T}{\partial z^2}\right) - \left(u\frac{\partial T}{\partial x} + w\frac{\partial T}{\partial z}\right) + \frac{2\,A^{-\frac{1}{n}}\,\dot{\varepsilon}^{\frac{1+n}{n}}}{\rho\, C}, \tag{2}$$

where χ and C are the thermal diffusivity and the specific heat capacity, respectively. The terms in the first and in the second brackets respectively define the heat transfer due to heat diffusion and due to ice advection. The last term is associated with strain heating.

In this model it is suggested that the ice surface temperature at the Academy of Sciences Ice Cap varies with an elevational gradient of temperature changes, which is equal to about $6.5\ ^0\text{C}/\text{km}$. Hence, the ice surface temperature distribution along the flow line is defined by the temperature history at the summit $T_{s0}(t)$ and by the elevational changes, and it is expressed as

$$T_s(x,t) = T_{s0}(t) + \theta_T\left(h_s(0) - h_s(x)\right), \tag{3}$$

where θ_T is the elevational gradient. Therefore, equation (3) provides the boundary condition on the ice surface. However, it should be noted that equation (3) does not account firn warming through refreezing meltwater.

The boundary condition at the ice base is defined by the geothermal heat flux and by the heating due to the basal friction, and it is expressed as [3], [4]

$$\frac{\partial T}{\partial z} = -\frac{1}{k}\left(Q + (\sigma'_{xz})_b u_b\right), \quad (4)$$

where k is the thermal conductivity.

The boundary conditions at the ice (ice-shelf) terminus and at the ice-shelf base are defined by sea water temperature, which is considered as $-2\,^{\circ}\mathrm{C}$ in this study.

The ice thickness temporal changes along the flow line are described by the mass-balance equation [3], [4]:

$$\frac{\partial H}{\partial t} = M_s - M_b - \frac{1}{b}\frac{\partial(\bar{u}\, b\, H)}{\partial\, x}, \quad (5)$$

where $\bar{u}$ is the depth-averaged horizontal velocity, M_s is the annual surface mass balance, and M_b is the melting rate at the ice base.

The mass-balance equation requires two boundary conditions at the summit and at the ice terminus. The first condition at the ice cap summit implies that $\partial h_s/\partial x = 0$. The second condition applied in the ice terminus originates from the fact that the ice thicknesses in the ice shelf along the flow line attain a constant value at the terminus.

2.4. Grounding line evolution

In the model the grounding line position is defined from the hydrostatic equilibrium [20]-[22]. That is, since sea water flow under ice shelf is not considered in the model and, hence, the pressure in equations (10)-(11) from [21] is equal to hydrostatic pressure, and the grounding line position is at the location where

$$-\rho_w\, h_r = H \quad (6)$$

and h_r is the bedrock elevation, ρ_w is the water density.

3. Results of the prognostic experiments

The main input data along with flow-line profiles for the prognostic experiments, namely, the surface mass balance, are adopted from [23]. For instance, figure 7 of [24] shows the elevational mass-balance distribution along the C–C′ flow line, i.e., it shows how the surface mass balance changes with elevation in the C–C′ direction [23]. For the B–B′ and D–D′ flow lines, the elevational mass-balance distributions are qualitatively the same [23]. In the prognostic experiments that have been carried out, the mass balance is considered as time-independent. That is, the elevational mass-balance distributions are kept unchanged for the considered time period in the future. Thus, we intend to assess the maximum ice thickness in the ice streams in the future, because the forecasts implemented with the time-independent surface mass balance, don't imply a future global warming and, so, they don't suggest a future decreasing of the surface mass balance M_s in equation (5). Similarly, the ice surface temperature is suggested to be time-independent but dependent on elevation, i.e., according to equation (3), it is changed with elevation with a constant value of $T_{s0}(t)$. From the borehole temperature measurements, the present ice surface temperature at the summit is about $-7.2\,^{\circ}\mathrm{C}$. The initial ice temperatures applied in the prognostic experiments are shown in figure 5 of [24].

Despite that future warming scenarios are not included into the prognostic experiments, the modeled ice cap response to the present environmental impact, which is reflected in the elevational mass-balance distribution [23], reveals that the ice thicknesses gradually diminish along all the three flow lines. Figure 1 shows the modeled successive ice surfaces divided into 50-year time intervals for the B–B′, C–C′, and D–D′ profiles, respectively. The prognostic experiments are performed by applying a rectangular ice-shelf geometry (figure 1). The cumulative impact of sea water, surface mass balance, and ice flow changes in the glacier has produced the future modeled ice shelve geometries (figure 1; figures 8-10 of [24]).

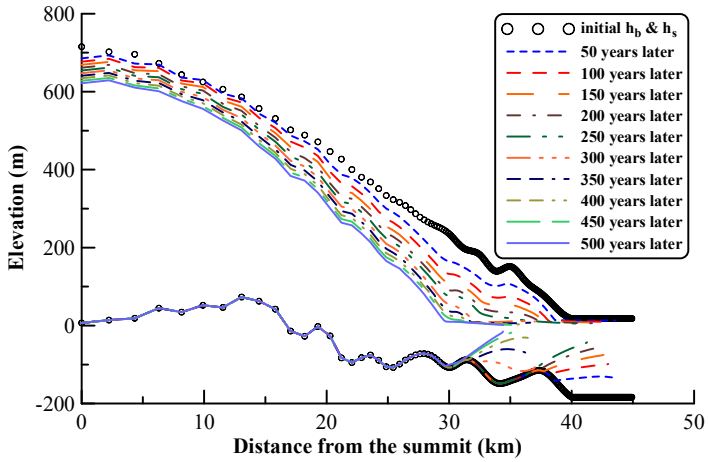

Figure 1 (a)

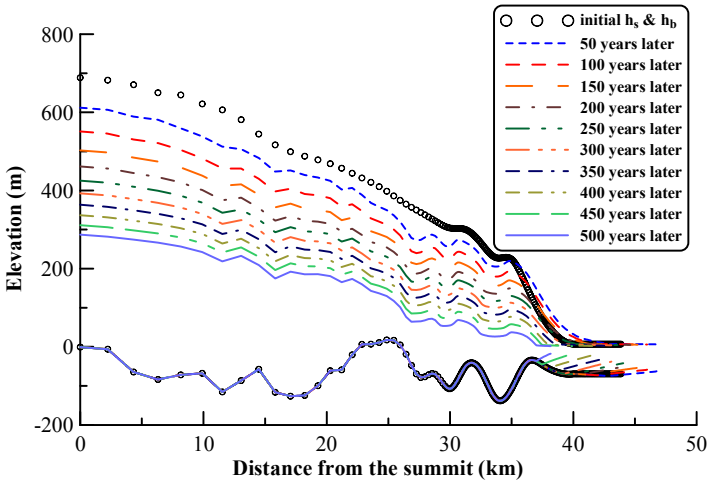

Figure 1 (b)

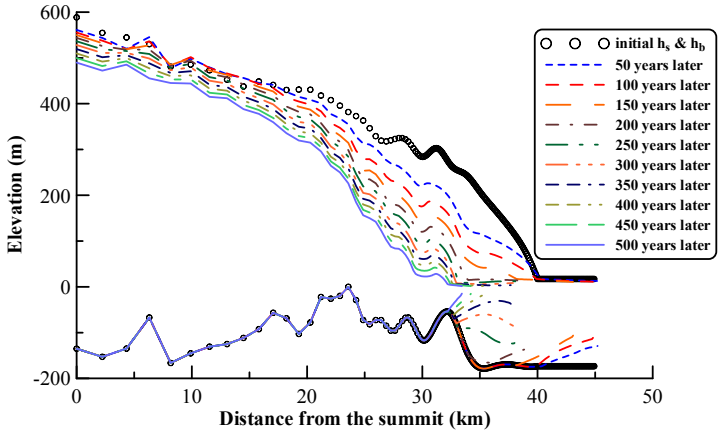

Figure 1 (c)

Figure 1. (a) The modeled successive B-B' cross-section geometries separated by 50-year intervals from the present to the future 500 years later. **(b)** The modeled successive C-C' cross-section geometries separated by 50-year intervals from the present to the future 500 years later. **(c)** The modeled successive D-D' cross-section geometries separated by 50-year intervals from the present to the future 500 years later.

The ancillary black circles in figure 1 are aligned with the grid nodes and, thus, they show the spatial resolution, at which the prognostic experiments have been implemented. The spatial resolution is irregular and it decreases from about $2 \cdot 10^3$ m at the summit to about 10^2 m in the grounding line vicinity and in the ice shelf. The spatial grid is considered unchangeable throughout the period of the modeling.

The grounding line history, i.e., grounding line retreat or advance, specifically reflects the growing or diminishing ice mass, i.e., the history is an indicator of the glacier evolution. The grounding line retreats (a) along the B–B′ flow line from ~40 km to ~30 km (figure 11 (a) of [24]), (b) along the C–C′ flow line from ~43 km to ~37 km (figure 11 (b) of [24]), and (c) along the D–D′ flow line from ~41 km to ~32 km (figure 11 (c) of [24]) considering a time period of 500 years.

Furthermore, the results of the prognostic experiments can be likewise treated suggesting a changes in the friction coefficient. The glacier terminus, currently fast flowing and therefore at pressure melting, becomes eventually frozen to the ground – ice thickness insufficient to insulate from cold atmosphere and reduced driving stress and strain heating. So basal friction coefficients could change drastically, given the simulated changes in glacier geometry.

The ice flow velocities in the ice streams decrease with time and this trend diminishes the outgoing ice fluxes in the future (figure 12 of [24]). Figure 13 of [24] shows the future history of the overall outgoing ice flux, i.e., it is the sum of the three future modeled outgoing ice fluxes obtained for B–B′, C–C′ and D–D′ ice streams.

There are small peaks that periodically disturb main historical trends of the three outgoing ice fluxes (figure 12 of [24]). Every peak reflects ice calving at the ice-shelf terminus. Similarly, the ice calving provides a sudden change in the value of the outgoing ice flux ($\bar{u} H b$) due to a sudden change in the ice thickness (H) at the terminus. Considering a complex environmental impact on ice shelves [25], from the mathematical point of view it can be suggested that the calving processes are described by a stochastic model. Hence, the overall annual (or decadal) sizes of the anticipated ice debris can be described by a frequency distribution function. In the model In the model the periodic calving of equal-size debris is considered, i.e., δ-function is considered as the frequency distribution function.

In this model the both ice-shelf length and ice-shelf thickness at the terminus are considered as the variables that should satisfy a certain conditions. If the ice-shelf length exceeds a value l_{cr} (the parameter of the model) or the ice-shelf thickness beside the terminus becomes smaller than a value H_{cr}, then the calving of the appropriate part of ice occurs in the model. To investigate the impact of the parameters on the results of the modeling, the parameters were varied in a series of the experiments. However, the simulation reveals that the mass balance, friction coefficient, ice temperature have the main impact to the assessment of the grounding line retreat derived by the modeling.

4. Conclusions

The modeled present ice temperatures (figure 5 of [24]) are qualitatively the same in the three cross-sections. There are resembling zones of relatively cold ice that can be distinguished in the modeled temperatures in the middle of the cross-sections. These cold ice zones reflected the surface temperature minimum about 150–200 years ago in the inverted past temperature history [18], [19]. This surface temperature minimum corresponds to an event that is known as Little Ice Age.

The inversions of the friction coefficient performed for the three cross-sections can be interpreted as follows. The two levels that are evidently distinguished in the inverted friction coefficient distributions (figure 6 of [24]) can be explained by changing the physical properties of the bedrock along the flow lines. Similarly, the large values of the friction coefficient at 0 km < x < 20 km justify the rock-type bottom where ice is frozen to the bed (the ice temperature at 0 km < x <20 km is lower than the melting point). The lower values of the friction coefficient at 25 km < x <40 km presumably indicate the existence of the till layer (or the sandy layer) at the bottom. Specifically, the till layer provides the basal ice sliding [26]-[33].

The prognostic experiments carried out with the reference mass balance [23] show that the grounding line has been retreated at about 10 km in the three ice streams considering a time period of 500 years. Similarly, the grounding line retreats (a) along the C–C′ flow line from ~43 km to ~37 km (the distance from the summit), (b) along the B–B′ flow line from ~40 km to ~30 km, and (c) along the D–D′ flow line from ~41 km to ~32 km considering a time period of 500 years and assuming time-independent mass balance. In the experiments, the ice flow velocities in the ice streams decrease with time due to (a) diminishing of the ice thicknesses and (b) retreating of the grounding lines from the sliding zones toward the zones where ice is frozen to the bed. Thus, the maxima of the ice flow velocities in the ice streams decrease from ~80–120 m/a to ~20–30 m/a. These trends in the ice flow velocities diminish the outgoing ice fluxes and as a result diminish the overall ice flux (figure 13 of [24]). The modeled evolution of the ice streams is in agreement with observations of ice mass loss on Severnaya Zemlya archipelago [16].

Acknowledgements. Authors are grateful to Prof. J.A. Dowdeswell et al. for the data that have been used in the manuscript. Authors are grateful to Prof. F. Pattyn for the useful comments to the manuscript. Authors are grateful to Dr. T. Dunse for the reviewing the manuscript.

References

[1] Dowdeswell J A, Bassford R P, Gorman M R, Williams M, Glazovsky A F, Macheret Y Y, Shepherd A P, Vasilenko Y V, Savatyugin L M, Hubberten H W and Miller H 2002 Form and flow of the Academy of Sciences Ice Cap, Severnaya Zemlya, Russian High Arctic *J. Geophys. Res.* **107** 1-15

[2] Colinge J, Blatter H 1998 Stress and velocity fields in glaciers: Part I. Finite difference schemes for higher-order glacier models *J. Glaciol.* **44** 448–456

[3] Pattyn F 2000 Ice-sheet modeling at different spatial resolutions: focus on the grounding zone *Ann. Glaciol.* **31** 211-216

[4] Pattyn F 2002 Transient glacier response with a higher-order numerical ice-flow model *J. Glaciol.* **48** 467-477

[5] Konovalov Y V 2012 Inversion for basal friction coefficients with a two-dimensional flow line model using Tikhonov regularization *Research in Geophysics* **2:e11** 82-89

[6] MacAyeal D R 1992 The basal stress-distribution of Ice Stream-E, Antarctica, inferred by control methods *J. Geophys. Res. Solid Earth* **97** 595-603

[7] Sergienko O V, Bindschadler R A, Vornberger P L, MacAyeal D R 2008 Ice stream basal conditions from block-wise surface data inversion and simple regression models of ice stream flow: Application to Bindschadler Ice Stream *J Geophys. Res.* **113** 1-11

[8] Arthern R and Gudmundsson H 2010 Initialization of ice-sheet forecasts viewed as an inverse Robin problem *J. Glaciol*. **56** 527-533

[9] Gagliardini O, Jay-Allemand M, Gillet-Chaulet F 2010 Friction distribution at the base of a surging glacier inferred from an inverse method *AGU Fall Meeting* C13A-0540 (San Francisco CA USA Dec. 13-17).

[10] Habermann M, Maxwell D A, Truffer M 2010 A principled stopping criterion for the reconstruction of basal properties in ice sheets *AGU Fall Meeting* C21C-0556 (San Francisco CA USA Dec. 13-17)

[11] Morlighem M, Rignot E, Seroussi H, Larour E, Ben Dhia H and Aubry D 2010 Spatial patterns of basal drag inferred using control methods from a full-Stokes and simpler models for Pine Island Glacier, West Antarctica *Geophys. Res. Lett.* **37** L14502

[12] Jay-Allemand M, Gillet-Chaulet F, Gagliardini O, Nodet M 2011 Investigating changes in basal conditions of Variegated Glacier prior to and during its 1982-1983 surge *The Cryosphere* **5** 659-672

[13] Larour E, Seroussi H, Morlighem M, Rignot E 2012 Continental scale, high order, high spatial resolution, ice sheet modeling using the Ice Sheet System Model (ISSM) *J. Geophys. Res.*

117 1-20
[14] Sergienko O V and Hindmarsh R C A 2013 Regular patterns in frictional resistance of ice-stream beds seen by surface data inversion *Science* **342(6162)** 1086–1089
[15] Tikhonov A N, Arsenin V Ia 1977 *Solutions of ill posed problems* (Washington: Winston & Sons)
[16] Moholdt G, Wouters B, Gardner A S 2012 Recent mass changes of glaciers in the Russian High Arctic *Geophys. Res. Lett.* **39** L10502
[17] Cuffey K and Paterson W S B 2010 *The physics of glaciers* 4th ed (Butterworth-Heineman, Elsevier).
[18] Nagornov O V, Konovalov Y V, Tchijov V 2005 Reconstruction of past temperatures for Arctic glaciers subjected to intense subsurface melting *Ann. Glaciol.* **40** 61-66
[19] Nagornov O V, Konovalov Y V, Tchijov V 2006 Temperature reconstruction for Arctic glaciers *Palaeogeogr. Palaeoclimatol. Palaeoecol.* **236** 125-134
[20] Schoof C 2007 Ice sheet grounding line dynamics: Steady states, stability, and hysteresis *J. Geophys. Res.* **112** 1–19
[21] Pattyn F, Schoof C, Perichon L, Hindmarsh R C A, Bueler E, de Fleurian B, Durand G, Gagliardini O, Gladstone R, Goldberg D, Gudmundsson G H, Huybrechts P, Lee V, Nick F M, Payne A J, Pollard D, Rybak O, Saito F and Vieli A 2012 Results of theMarine Ice Sheet Model Intercomparison Project, MISMIP *The Cryosphere* **6(3)** 573–588
[22] Seroussi H, Morlighem M, Larour E, Rignot E, Khazendar A 2014 Hydrostatic grounding line parameterization in ice sheet models *The Cryosphere* **8** 2075–2087
[23] Bassford R P, Siegert M J, Dowdeswell J A, Oerlemans J, Glazovsky A F and Macheret Y Y 2006 Quantifying the Mass Balance of Ice Caps on Severnaya Zemlya, Russian High Arctic I: Climate and Mass Balance of the Vavilov Ice Cap *Arctic, Antarctic, and Alpine Research* **38 (1)** 1-12
[24] Konovalov Y V, Nagornov O V 2015 Two-dimensional prognostic experiments for fast-flowing ice streams from the Academy of Sciences Ice Cap: future modeled histories obtained for the reference surface mass balance *Earth Syst. Dynam. Discuss.* **6** 2211–2242
[25] Bassis J N, Fricker H A, Coleman R, Minster J-B 2008 An investigation into the forces that drive ice-shelf rift propagation on the Amery Ice Shelf, East Antarctica *J. Glaciol.* **54** 17-27
[26] Engelhardt H F, Harrison W D, and Kamb B 1978 Basal sliding and conditions at the glacier bed as revealed by bore-hole photography *J. Glaciol*. **20(84)** 469-508
[27] Engelhardt H F, Kamb B, Raymond C F, and Harrison W D 1979 Observation of basal sliding of Variegated Glacier, Alaska *J. Glaciol.* **23(89)** 406-407
[28] Boulton G S 1979 Processes of glacier erosion on different substrata *J. Glaciol.* **23(89)** 15-38
[29] Boulton G S and Jones A S 1979 Stability of temperate ice caps and ice sheets resting on beds of deformable sediment *J. Glaciol.* **24(90)** 29-43
[30] MacAyeal D R 1989 Large-scale ice flow over a viscous basal sediment: theory and application to ice stream B, Antarctica *J. Geophys. Res.* **94** 4071–4088
[31] Engelhardt H and Kamb B 1998 Basal sliding of Ice Stream B, West Antarctica *J. Glaciol.* **44(147)** 223-230
[32] Iverson N R, Hooyer T S, Baker R W 1998 Ring-shear studies of till deformation: Coulomb-plastic behavior and distributed strain in glacier beds *J. Glaciol.* **44** 634–642
[33] Tulaczyk S, Kamb W B, Engelhardt H F 2000 Basal mechanics of Ice Stream B, West Antarctica I. Till mechanics *J. Geophys. Res.* **105** 463–482